

# Filtration Processes and Design of Filters

Antonio F. Miguel

**Abstract** The process of filtration is widely used from domestic use to industry. Filters are used in vacuum cleaners and air conditioning systems but also in a wide variety of critical applications such as in the nuclear, electronic, aerospace, pharmaceutical and medical fields. How filtration process takes place? What kinds of filters are available? How to design good filters? This chapter is devoted to filtration theory, design and international standards for efficient air filters. It represents an attempt to bridge a gap in the literature by presenting an integrated view of the current state of art in this fascinating field of filtration.

**Keywords** Filtration • Aerosol • Porous media • Filters • Design

## 1 Aerosols: Characteristics and Classification

Aerosol consists of solid or liquid particles suspended in a gas. Dust, smoke, mists, fog, haze, and smog are various forms of common aerosols. The size of air molecules is about 0.3 nm and the mean free path (average distance a molecule travels between collisions) is about 70 nm, but aerosol sizes are the result of several competing processes such as the condensation, sedimentation, agglomeration, impaction, etc. In terms of the size and formation mechanism are classified into fine and coarse particles (Fig. 1). Fine particles are composed of nuclei and larger conglomerates of material that is accumulated. The nuclei mode (size < 0.1  $\mu\text{m}$ ) consists primarily of combustion particles emitted directly into the atmosphere and particles formed in the atmosphere by gas-to-particle conversion. They have relatively short lifetimes and coagulate rapidly. These

---

A. F. Miguel (✉)

Department of Physics and Geophysics Center CGE, University of Evora, Evora, Portugal  
e-mail: afm@uevora.pt

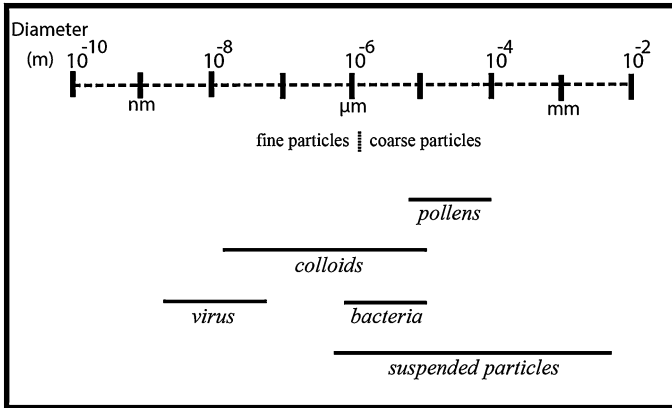


**Fig. 1** Aerosol particle size distribution

coagulated nuclei-mode particles, together with smog particles constitute the accumulation mode ( $0.1 \mu\text{m} < \text{size} < 2 \mu\text{m}$ ). Coarse particles (size  $> 2 \mu\text{m}$ ) consists of mechanically generated anthropogenic particles such as those from agriculture and surface mining, and windblown dust. Biogenic particles (e.g. viruses, intact bacterial cells, fungal cells, plant pollen grains, and insects' debris) are also available in the atmosphere mainly in coarse mode [23]. Particles larger than  $100 \mu\text{m}$  have a short lifetime in the atmosphere because they readily settle out. Additionally, a common aerosol particle size distribution is the lognormal distribution which usually fits those from a single source.

Aerosol particle concentration impairs visibility and affects air quality. They can be carried over long distances by wind and then settle on ground and water, or breathed in by people and animals. Aerosol particles are a primary component of the haze that obscures visibility in our cities. Some aerosols can contribute to acid rain issues (i.e., to make streams acidic, deplete nutrients in soil, damage of forests, farm crops, stone and other materials including monuments, etc.). Outdoor aerosol may also enter the buildings and may affect the indoor environments [45]. Aerosols are also generated inside the buildings during indoor activities such as cooking, heating, smoking, candles and incense burning, etc. Flea powder, aerosolized insecticides, cleaning products and indoor materials may also act as sources aerosols [56, 64].

Inhalable (i.e., particles smaller than  $100 \mu\text{m}$  are typically inhaled), thoracic (i.e., inhalable particles less than  $10 \mu\text{m}$  that can reach the thorax), and respirable particles (i.e., particles less than  $4 \mu\text{m}$ ), are likely to deposit in different regions of respiratory tract. Therefore, once breathed in, particles may reach the alveoli and settle, causing severe inflammation and may enter the bloodstream, circulating through all body. Epidemiological studies show that fine air pollution particles have a large impact on people health. The extent of this impact depends upon the aerosol concentration, chemical composition and exposure time. Cardiopulmonary

diseases (heart and lung diseases including asthma and bronchitis) are among the most important health effects [8, 50]. The effects are more pronounced in people who are not healthy.

The adverse effect of particulate air pollution on health has led to standards for levels of particulate matter in outdoor air [47, 48, 68]. PM10 stands for particulate matter up to 10  $\mu\text{m}$  in aerodynamic diameter which includes thoracic fraction of particles, and the 24 h standard for these particles is 150  $\mu\text{g}/\text{m}^3$  [47]. Evidence that small aerosols were particularly damaging has led to more stringent standards for levels of particulate matter. A new indicator (PM2.5) was then created for particulate matter up to 2.5  $\mu\text{m}$  in aerodynamic diameter (fine particles). The annual particles standard for PM2.5 is within the range of 12.0–13.0  $\mu\text{g}/\text{m}^3$  [47]. However, in people with asthma, even relatively low concentrations of PM2.5 air pollution worsen lung function [9]. Short-term exposure to PM2.5 also increases the risk for hospital admission for cardiovascular and respiratory diseases [11]. Authors [11] found that the largest association was for heart failure.

Not all aerosols have harmful effects on human health. Aerosolized medications have been used for centuries to treat some diseases. They play an important role in asthma and other lung complaints. There are also applications under development such as the inhalation of insulin to treat diabetes [71], treatment of lung diseases with aerosolized gene therapy (e.g., inhaled complementary DNA to treat Cystic Fibrosis) [18, 20] and vaccination via aerosol (candidates includes measles, influenza, rubella and anthrax) [32, 46]. In contrast to oral and injection therapies, the route of administration eliminates the potential for poor absorption and high metabolism in the gastrointestinal tract, eliminates losses in the liver, and the pain and discomfort that is associated to injection therapy.

## 2 Porous Media for Aerosol Filtration

Filtration is a very effective and common method for aerosol removal. Particles are collected for air refinement or aerosol sampling. Filters are made in a variety of materials such as cellulose, Teflon, nylon, polyvinyl chloride, silver, quartz, etc. They can be classified according to their structure in porous membrane filters, packed-bed filters and fibrous filters [5, 65]. There is also a new class of filters of biologically-inspired design that deserves to be also included [39, 58].

Porous membrane filters consist of cellulose ester, polyvinyl chloride, and Teflon membranes with relatively uniform microstructure channels that allows the capture of particles transported by passing air. The porosity is less than 0.85 and thickness ranges from 0.05 to 0.2 mm. Their manufacture consists of polymer films that are bombard by neutrons followed by etching process. From this procedure results an array of cylindrical holes (pores) of uniform diameter perpendicular to the surface of the filter. Within this class of filters, capillary porous membrane filters (porosity between 0.05 and 0.10) are particularly suitable for collecting particles for observation in the microscope.

Fibrous filter media composed by fibres or filaments of natural or synthetic materials have been used extensively in filtration [65]. A variety of these filters made of cellulose, polymer and quartz fibres are available, having porosities ranging from 0.55 to 0.99 and thicknesses up to 0.5 mm. These filters vary in efficiency and effectiveness.

Fibres or filaments spun into a continuous yarn results in a woven media filter. Single filaments, multifilament yarns, or twisted staple yarn characterized these media. The nature of the basic fibre or filament, and the way in which the yarns are woven together determine the properties of the filter. The regular structure and the relative strength, both mechanical and chemical, make woven materials valuable as filtration media. There are also woven filter media composed by a wide variety of wire meshes of either ferrous or non-ferrous metals. They are used to remove very large, harsh particulate under extreme conditions of temperature, corrosion and abrasion.

The so-called non-woven media filters are made up from a random array of fibres or filaments, held together to form a flexible sheet [28, 69]. They can be felts (i.e., rely on the characteristics of the fibre to provide mechanical integrity or on mechanical processing to create a fabric) and bonded fabrics (i.e., they use additional adhesive material to hold the fibres together). Non-woven filters are porous fabrics with greater flexibility and versatility.

Packed-bed filters consist of a fine granules, usually glass, quartz, metal, and activated charcoal. The porosity is higher than 0.26 [60]. Particles are collected on the surface of the beds and may be removed by washing, volatilization or using solvents. Packed-bed filters are particular suitable for corrosive aerosols at high temperature. Materials such as activated carbon, fuller's earth and ion exchange resins are also used for promoting adsorption of gaseous pollutants. Deep-bed filtration is used for gas and liquid filtration.

Biofilters are reactors for the conversion of contaminated air into harmless products of carbon dioxide, water and mineral salts. The contaminated air is passed through a bed of porous moist medium, and the contaminants are adsorbed to the medium surface where they are degraded by the microorganisms in the medium [51, 63].

Filters found in living structures are innately selective: the relevant bio-structure controls the migration of particular species through it. One of examples is the lung that filters the air that we breathe constantly with high efficiency. The adherence to lung design (i.e., T-shaped and tree-shaped design) for an enhanced performance is proposed by different authors [27, 33, 39]. Recently, the T-shaped designs for particle removal was studied by Serrenho and Miguel [58].

### 3 Manufacturing Standards for Filters

By the end of the 1940's, deep beds of graded granular coke were used for radioactive material at "Hanford Works V" (which was part of Manhattan

Project), when high activity levels were detected in particulate form [13, 30]. These filters, both used at Hanford and Savannah River sites, operated at a superficial face velocity of 0.03 m/s, and had collection efficiencies of 99.7 % for particles greater than 0.5 μm [16]. High efficiency filters for treating reactor effluent gases were also mounted at Oak Ridge National Laboratory, Tennessee [66]. The system contained fibreglass prefilters with an efficiency of 99.9 % for particles greater than 0.1 μm. These filters were known as super-interception, and super-efficiency filters due to their high retention efficiency for small particles. Later, they were termed as “High Efficiency Particulate Air” filters (HEPA) by Gilbert [19].

In the search towards standard manufacturing and test criteria for filters, HEPA filters were defined as having a retention efficiency of 99.95 % for particles greater than 0.3 μm and airflow resistance (clean filter) up to 249 Ns/m<sup>3</sup> [1, 70]. This specific particle size criterion comes probably from the results obtained from Langmuir’s studies [29]. These studies consider only interception and diffusion mechanisms of particles removal, and obtained minimum filter efficiency for particle with 0.3 μm in diameter. Subsequent studies confirmed a minimum filterable diameter, but also that it depends on filtration mechanisms involved [36, 65]. These mechanisms will be described in next the section.

Ultra Low Penetration Air (ULPA) filters is another class of filters which their efficiency is defined for particles in the 0.1 μm range, that is the minimum filterable particle size for currently HEPA filters operating at their design airflow rate.

In summary, international standards for submicrometer particles distinguish among HEPA (with five classes) and ULPA (with 3 classes) filters (Table 1).

Today, HEPA and ULPA filters satisfy the high demands for air quality in various technology industries, such as aerospace, pharmaceutical, processing, electronics, nuclear fuels and nuclear power but also in hospitals and our buildings.

**Table 1** HEPA and ULPA filters characteristics according to the Comité Européen de Normalisation (CEN classification) [36]

Filter	EN 1822-1 filters class	Efficiency (%) <sup>a</sup>
HEPA	H10	85
	H11	95
	H12	99.5
	H13	99.95
	H14	99.995
ULPA	U15	99.9995
	U16	99.99995
	U17	99.999995

<sup>a</sup> Major particle penetration size—integral efficiency (mean value of all local efficiencies measured over the filter’s face area.)

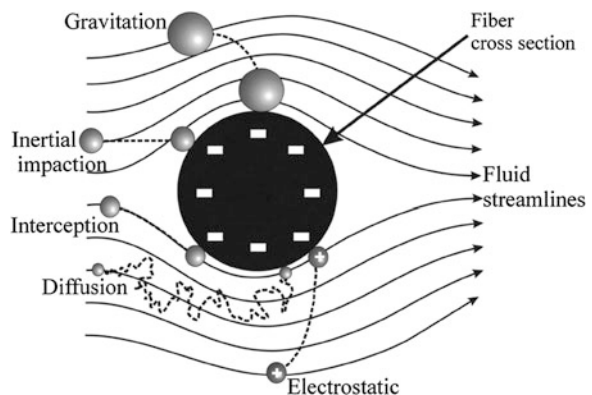
## 4 Particle Deposition Mechanisms in Filters

Filter media may retain particles at surface (surface filtration) and within the structure of the medium (depth filtration). Particles larger than the sizes of the filter pores deposit on the medium surface but particles smaller than the pore sizes deposit generally within the filter.

There are several mechanisms that govern the deposition of particles in filters (Fig. 2). When a particle following its fluid movement streamline comes in contact with the filter medium and becomes attached to it, the mechanism is known as interception. This takes place when a particle comes within a distance from the filter medium (i.e., fibre, bed, etc.) which is less than or equal to, the particle radius. Another possibility is when particles deviate from fluid streamlines: this greatly enhances the probability of hitting the fibre or bed and remain there. The deviation from streamlines is caused by different mechanisms:

1. Inertial impaction: the inertia of the particle that is carried by the fluid stream depends on its mass and velocity. When a particle is unable to adjust to the fluid stream turns and it continues on its previous path, it can be collected by the filter medium. The effectiveness of inertial impaction improves with the increasing particle mass and velocity and the decreasing particle size.
2. Gravitation: The settling of particles is due to the gravity, and is especially important where there are very heavy particles and very slow fluid velocities.
3. Diffusion: small particles in random directions (Brownian motion), instead of following fluid streamlines, can come in contact with the filter medium and remain there.
4. Electrostatic: experimental evidences indicated that both atmospheric particles and filter media possess electrical charges. If particles and the filter medium have charges of opposite signs, electrostatic forces arise from the Coulomb interactions between these charges, and particles come in contact with the filter medium and may remain there.

**Fig. 2** Schematic representation of particle deposition on a collector [36]



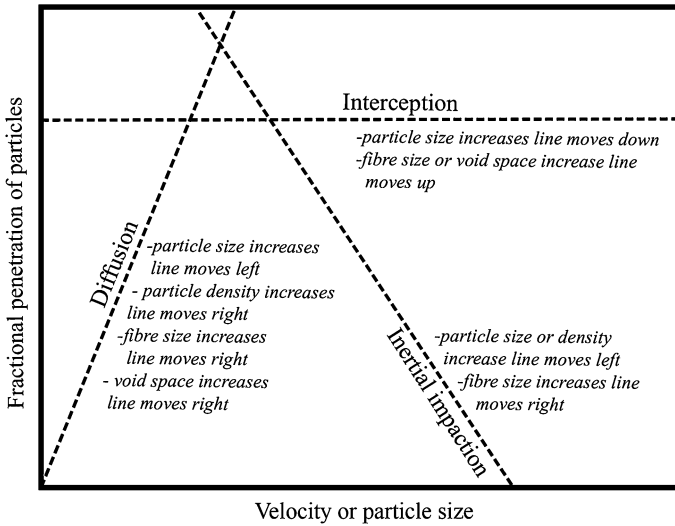


**Fig. 3** Influence of deposition mechanisms on the fractional penetration of particles-velocity curve [36]

Notice that the all five of the above-mentioned collection mechanisms are taking place simultaneously. Therefore, the collector-element efficiency,  $\eta$ , depends on the partial efficiencies of each aerosol capture mechanisms and can be obtained from

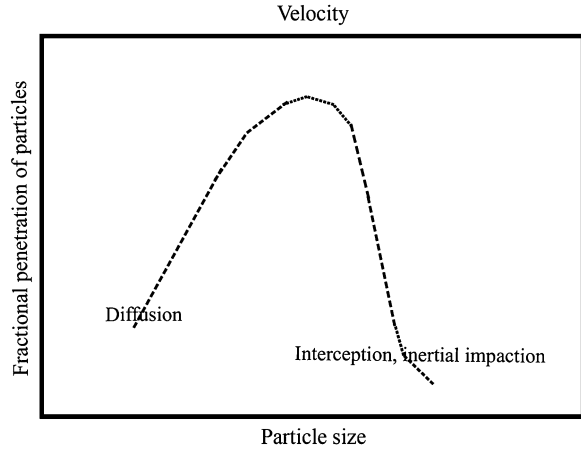
$$\eta = 1 - (1 - \eta_r)(1 - \eta_I)(1 - \eta_D)(1 - \eta_G)(1 - \eta_{el}) \quad (1)$$

where  $\eta_r$ ,  $\eta_I$ ,  $\eta_D$ ,  $\eta_G$  and  $\eta_{el}$  are the partial efficiencies for the particle deposition due to the mechanisms of interception, inertial impaction, diffusion, gravitation and electrostatic, respectively. A comprehensive review of partial efficiencies in filters is provided by Bejan et al. [5].

The expected penetration of particles through the filter for a given filtration velocity is presented at Fig. 3. For the inertial impaction mechanism, increasing particle radius and density improves particle collection efficiency (penetration is less). For diffusion deposition mechanism, as the particle radius decreases the slope of the line decreases and the influence of this mechanism increases. Besides, the greater the open pores in the filter is, the fluid velocity in the pore space of the filter is less (i.e., pore fluid velocity is the ratio between the superficial filtration velocity and the porosity) and transit time is longer. Therefore, the contact between particle and filter medium is more likely and the filter efficiency increases. On the other hand, as pore size increases, the particle penetration increases for both the inertial impaction and direct interception.

The smallest penetration of particles (highest particle deposition) occurs for the large particles at high velocities and for the finest particles at low velocities (Fig. 4). There is an intermediate size range ( $\sim 0.1$  to  $2 \mu\text{m}$ ) where penetration has

**Fig. 4** Influence of particle size on the typical fractional penetration of particles [36]



a maximum. This range depends very much on the ratio between the particle size and the collector size [5, 65]. This maximum can be lightened by the existence of electrostatic forces (i.e., Coulomb interactions).

## 5 Particle Loading Performance of Filter Media

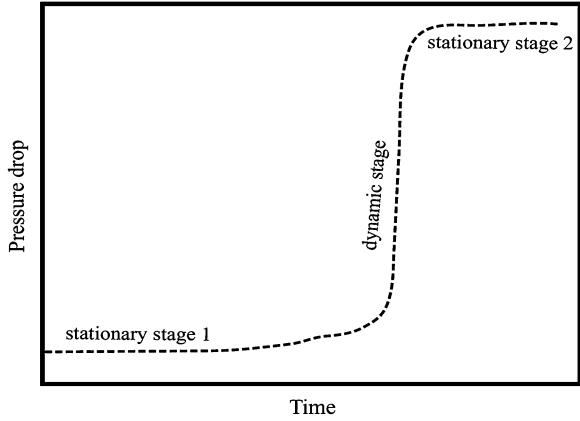
The choice of a filter is based upon fundamental attributes: the smallest particle sizes that the medium is able to retain, the dirt-holding capacity, the filter permeability to the fluid flow through it and the mechanical strength of filter medium. These attributes are closely related with the filter structure.

From the suspensions flow point of view, the filter should have high retention efficiency for particles (i.e., filter media should be characterized by low particle penetration), and a high permeability to fluid flow. In time, more and more solids are deposited in the filter leading to an increase of retention efficiency but also to a decrease in its ability to allow fluid to flow through it (i.e., reduction of filter permeability or increase of pressure drop). As a result, the pressure drop required for maintaining a constant airflow through the filter increases as the deposition process continues. The life of the filter depends greatly on this phenomenon. Therefore, the understanding of the filtration process over time, for given operating conditions, is crucial. In general, there are 3 stages that are represented in Fig. 5, [5]:

1. Particle deposition occurs in the filter structure. The filter efficiency and permeability is not very much affected in time (stationary stage 1).
2. Gradual deposition induces a gradual change of the structure of filter media. Particles start to deposit onto previous deposited particles, and pores start to clog. The filter efficiency increases and permeability decreases in time (dynamic stage).



**Fig. 5** Pressure drop through the filter in time and stages of filtration [42]



3. When approaching the clogging point, the filter efficiency and permeability no longer varies with time (stationary stage 2).

Particles deposited at the stationary stage 1 don't alter dramatically the internal structure of the filter (Fig. 6). During this stage, Zhao et al. [72] suggests that deposited particles only affect the collectors' sizes of the filter (e.g., fibres, beds, etc.). Denoting that the mass of particles collected per filter area is  $M_{pA}$ , the particle-loaded collector radius,  $r_c$ , and the filter solidity (or the volume fraction of the filter material),  $\alpha$ , are given by

$$r_c = r_{co} \left( 1 + \frac{M_{pA}}{\rho_c \alpha H} \right)^{1/2} \tag{2}$$

$$\alpha = \alpha_o \left( 1 + \frac{M_{pA}}{\rho_c \alpha H} \right) \tag{3}$$

where  $H$  is the filter thickness,  $\alpha_o$  is the filter solidity and  $r_{co}$  is the collector radius. The subscript  $o$  means clean filter (i.e., free of deposited particles).

Once the collectors' structure of the filter has evolved enough that no more particle collection occurs onto them, deposition onto previous deposited particles then takes place resulting in the formation of the particle cake (dynamic stage). In order to account for these circumstances, Emi et al. [14] suggest that, in fibrous filters, the collector-element efficiency evolution from clean filter is

$$\eta = \eta_o \left[ 1 + \left( \frac{M_{pA}}{0.316 b_{\eta 1} \eta_o u^{0.25}} \right)^{b_{\eta 2}} \right] \tag{4}$$

where  $\eta_o$  is the initial efficiency when the filter is clean, and  $b_{\eta 1}$  and  $b_{\eta 2}$  are, respectively, 0.0027 and 1.15 (filter mesh 200), or 0.0015 and 1.23 (filter mesh 325), and 0.0011 and 1.34 (filter mesh 500). The mesh size indicates the number of

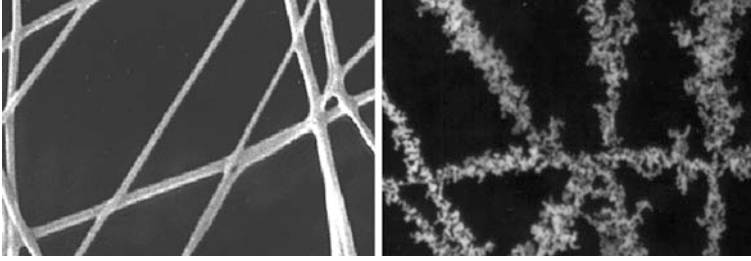


**Fig. 6** The effect of aerosol particle loading on fibrous filter (stationary stage 1)

fibres per inch in one of the directions (warp or weft). Besides, Jung and Tien [67] suggested that for granular filters the efficiency behaves as

$$\eta = \eta_o \left[ 1 + a_{\eta 1} \left( \frac{M_{pA}}{\rho_p H} \right)^{a_{\eta 2}} \right] \quad (5)$$

For experiments performed at  $0.0017 \leq St \leq 0.038$  and  $0.00172 \leq Ir \leq 0.008$ , the coefficients  $a_{\eta 1}$  and  $a_{\eta 2}$  are given by  $a_{\eta 1} = 0.095 St^{-1.48} Ir^{0.432} 10^{3a_{\eta 2}}$   $a_{\eta 2} = 0.442 St^{-0.347} Ir^{0.24}$ , where  $St$  is the Stokes number and  $Ir$  is the interception parameter (i.e., the ratio between the particle radius and the collector radius).

### 5.1 Filter Efficiency and Fractional Penetration

The smallest particles that are totally retained constitute the “absolute rating” of a filter. However, there are particles that are able to pass through the filter medium. Concentrations of particles measured upstream and downstream of the filter allows determining the fractional penetration of particles. Alternatively, filter efficiency  $\varphi$  is defined as

$$\varphi = 1 - \Pi = 1 - \frac{c_{dst}}{c_{ust}} \quad (6)$$

Here  $\Pi$  is the fractional penetration of particles (or simply penetration), and  $c_{ust}$  and  $c_{dst}$  are the concentrations of particles upstream and downstream of the filter, respectively. Research on aerosol filtration converges towards the idea that  $\Pi$  and  $\varphi$  depend, among other factors, on filter thickness, filter microstructure, particle characteristics and the mass of particles existing within the filter [5, 21, 65]. The penetration has an exponential dependence of the filter thickness,  $H$ , and an intrinsic quantity named characteristic filtration length,  $h$ , and can be expressed as [5, 61]

$$\Pi = \exp\left(-\frac{H}{h}\right) \quad (7)$$

The filtration length depends most notably on the microstructure of the filter and on particle size [10, 21]

$$h = \frac{2r_c}{s\alpha\eta} \quad (8)$$

where  $s$  is a coefficient that can be taken as equal to  $4/[\pi(1-\alpha)]$  for fibrous filters [17, 21], and equal to 1.5–1.88 for granular beds [12, 21, 57].

## 5.2 Filter Permeability and Pressure Drop

In accordance with Darcy's law, a suspension of particles moving with a slow, steady velocity, and the pressure drop through the filter are related by [5, 37, 40, 41]

$$\Delta p = \frac{\mu}{K} H u \quad (9)$$

Here  $u$  is the superficial velocity (the velocity within the filter—the intrinsic velocity—is related with the superficial velocity through the filter porosity),  $\mu$  is the viscosity and  $K$  is the intrinsic permeability. Darcy's law is used to define the permeability of the filter, provided that the viscosity is known.

In spite of its great applicability, the concept of permeability as a global quantity that characterizes the fluid flow, which grounds the validity of Darcy law, holds only for low values of the Reynolds number (i.e., creeping flow or Stokes flow). At sufficiently high Reynolds numbers, the flow through the filter is well approximated by a nonlinear approach [5, 37, 40]

$$\Delta p = \frac{\mu}{K} H u + \rho H \beta_\beta u^2 \quad (10)$$

or

$$\Delta p = \frac{\mu}{K} (1 + \beta_\beta K^{1/2} Re_K) H u \quad (11)$$

Here  $\beta_\beta$  is usually called the inertial parameter,  $Re_K$  is the Reynolds number based on the intrinsic permeability, and this phenomenological model is known as the as Darcy-Forchheimer equation. Experimental studies have shown that the transition from linear (Darcy flow) to nonlinear (Forchheimer or non-Darcy flow) regime occurs gradually as the Reynolds number increases [5]. For a Reynolds number based on the permeability,  $Re_K$ , the linear velocity term (Darcy law) is valid when  $Re_K$  is less than the 1–10 range.

For clean filters (i.e., free from particles), several relationships can be found in the literature to estimate  $K$  [5]. A variety of standard test methods are also available to measure permeability: ISO 9237 (fabrics including industrial fabrics for technical purposes, nonwovens and made-up textile; area for test  $2 \times 10^{-3} \text{ m}^2$ ; differential pressure  $2 \times 102 \text{ Pa}$ ), ASTM D737 (textile fabrics including woven, nonwoven blankets, napped, knitted, layered and pile fabrics; area for test  $38 \times 10^{-4} \text{ m}^2$  and differential pressure  $125 \text{ Pa}$ ), EDANA 140.1–81 (nonwovens media; area for test 2 to  $5 \times 10^{-3} \text{ m}^2$  and differential pressure  $125 \text{ Pa}$ ), etc. The inertial parameter  $\beta_\beta$  can be taken as equal to  $0.043(1-\alpha)^{-2.13} \text{ K}^{-1/2}$  for a fibrous filter [34], and equal to  $0.1429(1-\alpha)^{-3/2} \text{ K}^{-1/2}$  for a granular bed [15].

Models have been also developed to predict the loading behaviour of filters. For granular air filters, the permeability is described by [26]

$$K = \frac{K_o}{1 + a_{\kappa 1} \alpha_p^{a_{\kappa 2}}} \quad (12)$$

where  $\alpha_p$  is the packing fraction of particles (i.e., the volume of deposited particles per unit volume of filter) and  $a_{\kappa 1} = 0.348 \text{ St}^{-1.2} \text{ I}_r^{0.86} 10^{3a_{\kappa 2}}$  with  $a_{\kappa 2} = 3.51 \text{ St}^{-0.092} \text{ I}_r^{0.275}$  for  $0.0017 \leq \text{St} \leq 0.038$  and  $0.00172 \leq \text{Ir} \leq 0.008$ .

The permeability of fibrous filters is described by [6]

$$K = \frac{1}{16 \left( \frac{\alpha}{r_c} + \frac{\alpha_p}{r_p} \right) \left( \frac{\alpha}{r_c} + \frac{\alpha_p}{r_p} \right)^{1/2} \left[ 1 + 56(\alpha + \alpha_p)^3 \right]} \quad (13)$$

where  $r_p$  is the radius of the aerosols particles, and the filter solidity  $\alpha$  ranges from 0.006 to 0.3. For filters with lower solidity is given by

$$K = \frac{1}{16 \left( \frac{\alpha}{r_c} + \frac{\alpha_p}{r_p} \right) \left( \frac{\alpha}{r_c} + \frac{\alpha_p}{r_p} \right)^{1/2}} \quad (14)$$

The filtration of solid aerosol particles can occur under varying humidity conditions. A number of researchers [24, 25, 35, 42, 49] have carried out extensive laboratory tests to quantify this effect on the filter permeability as a function of particle hygroscopicity and size. Results have shown an increase in permeability with the increasing humidity for loading both with non-hygroscopic particles and hygroscopic particles below the deliquescent point. Miguel [35] proposed a model to account the effect of humidity on the permeability through its influence on the packing fraction of particles.

### 5.3 Filter Performance

Particle collection efficiency is often viewed as the primary performance indicator for filters. However, the filter permeability (or the pressure drop) is particularly

important due to safety and energy-saving issues [65]. Near clogging, there is an enormous increase in the pressure drop with the risk of filter damage and more energy required to operate the system. Therefore, an ideal filter is the one that has high efficiency arresting for particles with low pressure drop.

Filter performance (or filter quality) is often defined as the ratio of the negative logarithm of penetration to the pressure drop across the filter [65]. The figure of merit resulting from this definition has the advantage that it can be calculated directly from parameters that can be measured simply. Its drawback is that it is not a dimensionless factor. Its magnitude depends on the system used, and filters must be compared for specified filtration velocity, particle diameter and particle loading. To overcome this dimensional problem, filter performance is defined as the dimensionless ratio of collector-element efficiency to the friction factor for flow [5]

$$\Omega_{\eta fa} = \frac{\eta}{f_{fa}} \tag{15}$$

Here  $f_{fa}$  is the friction factor defined as  $\Delta p/0.5 \rho u^2$ . Miguel [35] based on  $\pi$ -theorem of Buckingham suggested as an alternative relationship for evaluating filter performance, the product of the number of particles caught per unit of filter area,  $N_{pA}$ , by the filter permeability

$$\Omega_{NK} = N_{pA} K \tag{16}$$

where  $N_{pA}$  is the number of particles caught per unit of filter area ( $M_{pA}/A_f \rho_p V_p$ ) and  $V_p$  is the average volume of each particle. Substituting Eqs. (12), and (14) into Eq. (16), yields

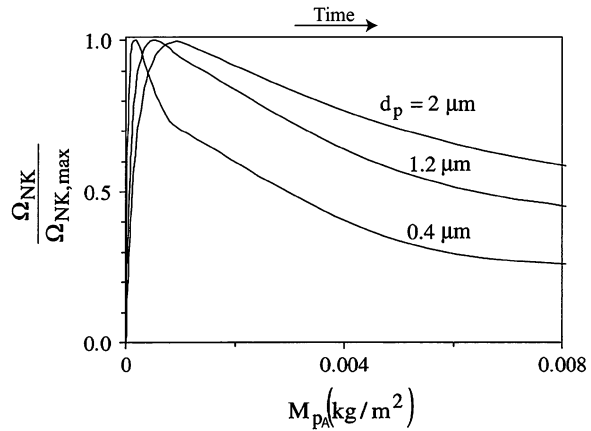
$$\Omega_{NK} = \frac{K_o M_{pA}}{\rho_p V_p (1 + a_{\kappa I} \alpha_p^{ak^2})} \tag{17}$$

$$\Omega_{NK} = \frac{M_{pA}}{16 \rho_p V_p \left( \frac{\alpha}{r_c} + \frac{\alpha_p}{r_p} \right) \left( \frac{\alpha}{r_c^2} + \frac{\alpha_p}{r_p^2} \right)^{1/2}} \tag{18}$$

Equations (17) and (18) are valid for granular filters and fibrous filters ( $\alpha < 0.006$ ), respectively. These equations allow a direct comparison of different filter media but also an estimation of the time evolution of the filter's performance which provides information regarding the need for filter replacement [35].

Figure 7 shows the ratio  $\Omega_{NK}/\Omega_{NK, \max}$  calculated for aerosol particles with several sizes. For each particle size there is a peak that corresponds to the maximum performance. After, the performance starts to decrease till reaching quasi-constant value, and the filter needs to be replaced. Notice that, when particle size increases the maximum value of  $\Omega_{NK}/\Omega_{NK, \max}$  drifts toward higher values of  $M_{pA}$  (or higher filtration time).

**Fig. 7** Ratio between the performance  $\Omega_{NK}$  and the maximum performance  $\Omega_{NK, \max}$  versus the mass of particles collected per fibrous filter area [35]



## 6 Modelling Particle Transport and Deposition

Some authors (e.g., [7, 53]) classified the filtration models into 3 classes: empirical or semi-empirical models (include empirical parameters obtained from observation), stochastic models (use probabilistic approaches) and network models (structure is usually conceptualized as random).

Computational fluid dynamics (CFD) is a very powerful tool for simulating particulate suspensions with deposition [22, 40]. Eulerian and Lagrangian methods may be applied to implement the task. The Eulerian method treats the particle phase as a continuum and develops its conservation equations on a control volume basis and in a similar form as that for the fluid phase. This perspective fits the view that the filtration process is a convective–dispersive phenomenon [44, 52, 61, 62]. The Lagrangian method considers particles as a discrete phase and tracks the pathway of each individual particle. In this perspective, the trajectory of particles can be predicted based on the force balance on the particle [2, 59, 67]. The choice of one of these methods depends decidedly of the objective and characteristics of the problem under examination.

There are some evidences that Lagrangian method perform a little better than the Eulerian method in predicting dispersion of pollutant around enclosures [55]. However, to date there are no comparative studies for filtration.

## 7 Fine Particle Filtration

### 7.1 Particle Deposition

Filtration of fine particles represents an example of transport in porous media which can be analyzed based on the convective–dispersive phenomenon [5, 44, 52,

61, 62]. One-dimensional transport of particles through a filter medium is governed by the dimensionless macroscopic equation

$$\frac{\partial \Phi^*}{\partial t^*} = \frac{\partial^2 C_z^*}{\partial z^{*2}} - \frac{Pe}{l_c^*} \frac{\partial C_z^*}{\partial z^*} \quad (19)$$

with

$$Pe = \frac{l_c u}{D}; t^* = \frac{Dt}{H^2}; C^* = \frac{C}{\rho_{air}}; \Phi^* = \frac{\Phi}{\rho_{air}}; l_c^* = \frac{l_c}{H}; z^* = \frac{z}{H}$$

where  $Pe$  is the Peclet number and relates convective to diffusive particulate mass transport,  $C_z$  is the concentration of particulate matter in the air stream,  $u$  is the fluid velocity,  $D$  is particle diffusion coefficient,  $t$  is the time,  $l_c$  is the characteristic length of filter collector's,  $H$  is the thickness of the filter,  $\rho_{air}$  is the air density and  $\Phi$  is the sink of particles in the filter (i.e., particles removed from the suspension), which for continuity reasons is  $\Phi = -\Phi_c - \Phi_p$ , where  $\Phi_c$  is the deposition onto the filter's collector and  $\Phi_p$  is the deposition onto previously deposited particles.

In order to solve this equation, a particle deposition rate approach is required. The rate of particle deposition onto the filter's collector and onto previously deposited particles is given by [44]

$$\frac{\partial \Phi_c^*}{\partial t^*} = \frac{Sh_c \vartheta^*}{l_c^*} C^* - \frac{k_e}{\alpha I_{pc}} \frac{Sh_c \vartheta^*}{l_c^*} \Phi_c^* \quad (20)$$

$$\frac{\partial \Phi_p^*}{\partial t^*} = \frac{k_e}{\alpha I_{pc}} \frac{Sh_p \vartheta^*}{l_c^*} \Phi_c^* \quad (21)$$

with

$$Sh = \frac{l_c \Theta}{D}; \vartheta^* = \vartheta H$$

Here  $Sh$  is the Sherwood number (represents the ratio of actual particulate mass transfer by a moving air stream to the particulate mass transfer that would occur by diffusion),  $I_{pc}$  is the aerosol particle interception parameter ( $= A_p V_c / A_c V_p$ ),  $A_p$  is the particle surface area,  $A_c$  is the filter collector surface area,  $V_p$  is the particle volume,  $V_c$  is the filter collector volume,  $\Theta$  is the particulate matter transfer coefficient,  $\vartheta$  is the specific surface area of the filter,  $\alpha$  is the solidity of a brand new (unloaded) filter, and  $k_e$  is the excluded surface area factor which has a theoretical minimum value close to 1.27.

The total deposit amount inside the filter  $\Phi^*$  is given by

$$\Phi^* = \frac{C_0^*}{1 - \frac{b_1}{b_2} \exp[(b_1 - b_2)L^*]} \left[ \frac{1}{b_1} [\exp(b_1 H^*) - 1] - \frac{b_1}{b_2^2} [\exp(b_2 H^*) - 1] \exp[(b_1 - b_2)H^*] \right] \left\{ \frac{Sh_p \vartheta^*}{l_c^*} t^* + \frac{\alpha I_{pc}}{k_e} \left( 1 - \frac{Sh_p}{Sh_c} \right) \left[ 1 - \exp\left( -\frac{k_e}{\alpha I_{pc}} \frac{Sh_c \vartheta^*}{l_c^*} t^* \right) \right] \right\} \quad (22)$$

Figure 8 shows the effect of dimensionless numbers (Pe, Shc, Shp) and geometrical parameter  $I_{pc}$  on  $\Phi^*/C_0^*$ . The plot shows that the amount of particles deposited increases with the Peclet number, being the effect stronger for  $0.1 < Pe < 50$ . Results also indicate that during the early stages of the filtration process deposition is mainly influenced by  $Sh_c$  but at later stages  $Sh_p$  becomes more important. Therefore, during the early stages deposition is favoured when  $Sh_c$  is larger than  $Sh_p$  but later deposition is enhanced when  $Sh_p$  is larger than  $Sh_c$ . Figure 8 also reveals that  $\Phi^*/C_0^*$  is influenced by  $I_{pc}$ , being, however this influence negligible when the filter approach the clogging. Notice that, when  $Sh_c$  is larger than  $Sh_p$  the increase of interception parameter favour deposition. The opposite effect occurs when  $Sh_c$  is smaller than  $Sh_p$ .

The time evolution of  $\Phi_c^*/C_0^*$ ,  $\Phi_p^*/C_0^*$  and  $\Phi^*/C_0^*$  is presented in Fig. 9. As expected, the plot shows that during the early stages of filtration the main contribution for the deposition is the fraction of particles deposited onto the filter's collector ( $\Phi_c^*$ ). After  $t^* \sim t_{cc}^* \sim 0.62$ , fibres or beds that constitute the filter become completely covered with particles. Therefore, particles have to deposit on particles already attached to these collectors.

Consider that the life time of a filter corresponds to filter close the clogging. If  $\phi$  is the void fraction of the filter (i.e., the porosity), the life time of the filter is reached for

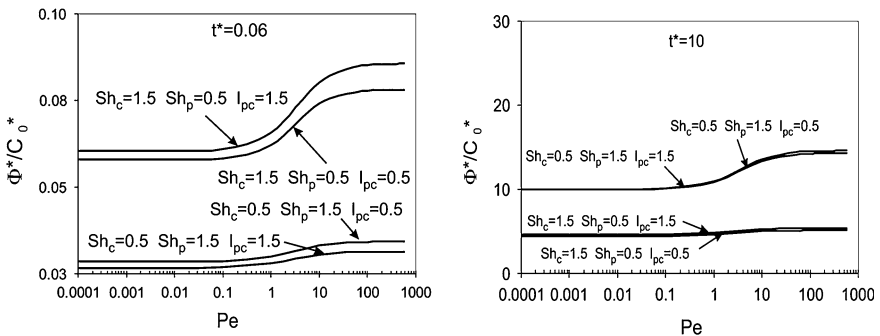
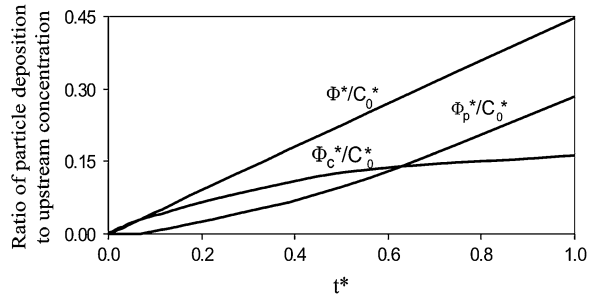


**Fig. 8** Effects of Peclet number, Sherwood number, interception parameter and filtration time upon  $\Phi^*/C_0^*$  ( $\alpha = 0.5$ ;  $k_e = 1.27$ ) [44]



**Fig. 9** Time evolution of  $\Phi^*/C_0^*$ ,  $\Phi_c^*/C_0^*$  and  $\Phi_p^*/C_0^*$   $C_0^*$  ( $\alpha = 0.5$ ;  $k_c = 1.27$ ) [44]



$$(\Phi^*)_{t_{life}^*} = \varphi \zeta \rho_p^* \quad (23)$$

where  $\zeta$  is the ratio between filter volume and particle volume, and  $\rho_p^*$  is the dimensionless particle density ( $\rho_p/\rho_{air}$ ). Eq. (23) may be the criterion to determine the life time of the filter.

## 7.2 Pressure Drop

The dimensionless form of Darcy's law reads (e.g., Miguel [35])

$$\Delta p^* = \frac{H^*}{K^* \text{Re}} \quad (24)$$

with

$$p^* = \frac{p}{\rho u^2}; \quad K^* = \frac{K}{l_c^2}; \quad H^* = \frac{H}{l_c}; \quad \text{Re} = \frac{\rho u l_c}{\mu}$$

For filters with porosities up to 0.8, based on the hydraulic radius theory of Carman-Kozeny

$$K^* = \frac{1}{45} \frac{\phi^3}{(1-\phi)^2} \quad (25)$$

and the pressure drop reads as [44]

$$\Delta p^* = 45 \frac{H^* (1-\phi)^2}{\text{Re} \phi^3} \quad (26)$$

with

$$\phi = \phi_0 - \zeta \frac{\Phi^*}{\rho_p^*}$$

and

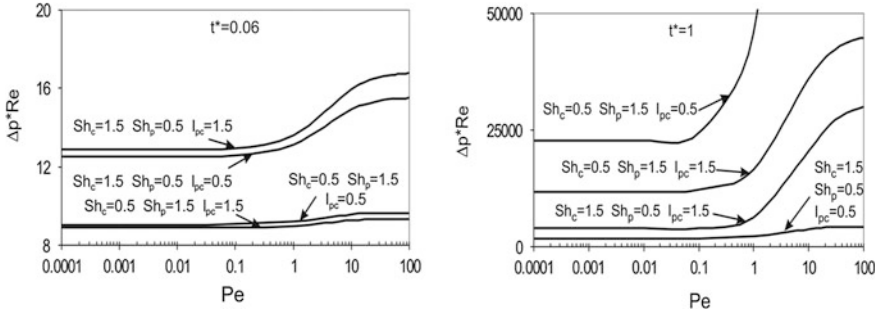


**Fig. 10** Effects of Peclet number, Sherwood number, interception parameter and filtration time upon  $\Delta p^*Re$  ( $\alpha = 0.5$ ;  $k_c = 1.27$ ) [44]

$$\begin{aligned} \varphi = \phi_0 - \frac{\zeta C_0^*}{\rho_p^* - \rho_p^* \frac{b_1}{b_2} \exp[(b_1 - b_2)H^*]} \left[ \frac{1}{b_1} [\exp(b_1 H^*) - 1] \right. \\ \left. - \frac{b_1}{b_2} [\exp(b_2 H^*) - 1] \exp[(b_1 - b_2)H^*] \right] \left\{ \frac{Sh_p \vartheta^*}{l_c^*} t^* \right. \\ \left. + \frac{\alpha I_{pc}}{k_e} \left( 1 - \frac{Sh_p}{Sh_c} \right) \left[ 1 - \exp\left( -\frac{k_e}{\alpha I_{pc}} \frac{Sh_c \vartheta^*}{l_c^*} t^* \right) \right] \right\} \end{aligned}$$

where  $\phi_0$  is porosity of a brand new (unloaded) filter and  $\zeta$  is the ratio between the filter volume and the particle volume.

The curve representing the variation of  $\Delta p^*Re$  with  $Pe$ ,  $Sh$  and  $I_{pc}$  is represented in Fig. 10. The plot reveals an increase of  $\Delta p^*Re$  with the Peclet number and this tendency is more noteworthy between 0.1 and 50. Initially  $\Delta p^*Re$  is enhanced if  $Sh_c$  is larger than  $Sh_p$  but at later stages the opposite occurs (i.e.,  $\Delta p^*Re$  is enhanced when  $Sh_p$  is larger than  $Sh_c$ ). This result stresses the importance of both  $Sh_c$  and  $Sh_p$  in the filtration process. In addition, when  $Sh_c$  is larger than  $Sh_p$  an increase of interception parameter favour pressure drop. The opposite effect occurs when  $Sh_c$  is smaller than  $Sh_p$ .

Notice also that, the tendency of variation of  $\Delta p^*Re$  with the Peclet and Sherwood numbers, as well as the interception factor is similar to  $\Phi^*/C_0^*$ . This is an expected result because the pressure drop through the filter is strongly dependent on the amount of particles deposited.

### 7.3 Filter Performance

Filter performance in terms of dimensionless quantities can be evaluated from the product of the number of particles caught per unit of filter area and the filter permeability (Eq. 16). In terms of dimensionless quantities it reads:

$$\Omega = \frac{\Phi^*}{\rho_p^* A_f^*} K^* \tag{27}$$

where  $\rho_p^*$  is the dimensionless particle density ( $\rho_p/\rho_{air}$ ) and  $A_f^*$  is the dimensionless filter area ( $A_f/l^2_c$ ). By combining Eq. (25) with (27), one obtains:

$$\Omega = \frac{1}{45 \rho_p^* A_f^*} \frac{\Phi^* \left( \phi_0 - \zeta \frac{\Phi^*}{\rho_p^*} \right)^3}{\left( 1 - \phi_0 + \zeta \frac{\Phi^*}{\rho_p^*} \right)^2} \tag{28}$$

where  $\Phi^*$  is obtained from Eq. (22).

The time variation of performance is shown in Fig. 11. This plot displays four different regions: an initial steep increase until it reaches a maximum (the peak), followed by a steep decrease, a transition range and an ending range of constant performance. This last range corresponds to filter close to clogging.

### 8 Deep-Bed Filtration

Deep-bed filtration refers to filtration through beds of granular or fibrous filter material. As the suspension travels through the filter, particles deposit at different depths on the filter grains.

There are some fundamental issues concerning packing of beds that remain elusive, including the precise effect of packing arrangements on flow of suspensions. The face-centered cubic packing is the way pack identical spheres together in the densest possible way (i.e., porosity of  $1-\pi/18^{1/2}$  ( $\sim 0.260$ ) and packing density  $\pi/18^{1/2}$ ). This arrangement found in cannonballs piled at war memorials or fruit arrangements was called the Kepler conjecture [31]. The packing structure can also be presented within different arrangements (e.g., cubic, hexagonal,

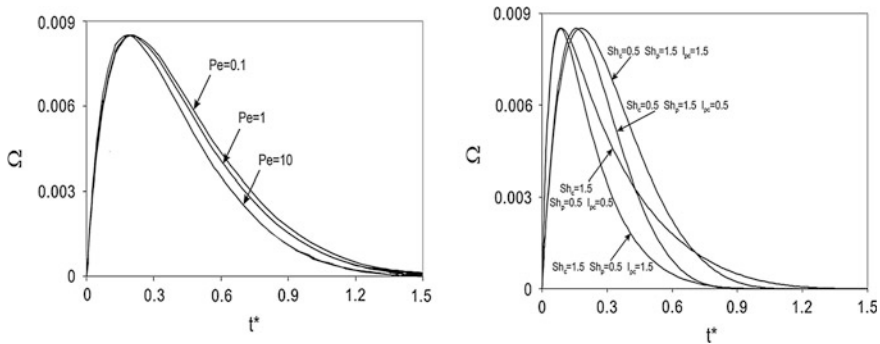


**Fig. 11** Effects of Pelet number, Sherwood number and interception parameter upon the time variation of filter's performance ( $\alpha = 0.5$ ;  $k_e = 1.27$ ) [44]



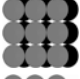
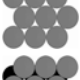
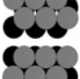
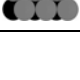
orthorhombic, etc.). In case of identical spheres, together in the densest possible way, the packing density of these structures varies between  $\pi/18^{1/2}$  (rhomboedric hexagonal or face-centered cubic) and  $\pi/6$  (simple cubic). Therefore, the packing arrangement is directly relevant to macroscopic key parameters such as the filter permeability and the fractional penetration of particles.

Serrenho and Miguel [60] performed CFD simulations to study fluid and suspension flows through 5 packing structures of fixed spheres: models SCU (simple cubic), FCC (face-centered cubic), ORT (orthogonal), HEX (hexagonal), RHE (rhomboedric hexagonal) and TET (tetragonal). These structures are constructed with spheres of same diameter and in a way that all have the same porosity (Table 2).

The flow pathlines that resulted from the 3D simulations ( $0.2 \leq Re \leq 40$ ) are depicted at Fig. 12. This figure shows differences between low and high Reynolds numbers: the predominant viscous forces in the momentum transport through the void geometry generates a more uniform “pathlines” velocities at  $Re = 0.2$ , whereas at  $Re = 40$  “channels” of air flow are generated due to the relevant contribution of inertial forces. Although all geometries having the same porosity the air flow coefficients are not the same (Table 3). The packing arrangements FCC and TET, RHE and ORT, and SCU and HEX present similar coefficients. SCU and HEX arrangements present the highest permeability and the lowest inertial coefficient.

Based on a Lagrangian approach, that considers particles as a discrete phase and tracks the pathway of each individual particle, the fractional penetration of

**Table 2** Ordered packing of spheres with same sphere diameter and porosity (packing density 0.42, porosity 0.52) [60]

Packing model		Arrangement
Simple cubic	SCU	
Face-centered cubic	FCC	
Orthogonal	ORT	
Hexagonal	HEX	
Rhomboedric hexagonal	RHE	
Tetragonal	TET	

**Fig. 12** Airflow pathlines within the packing arrangements (longitudinal section) [60]

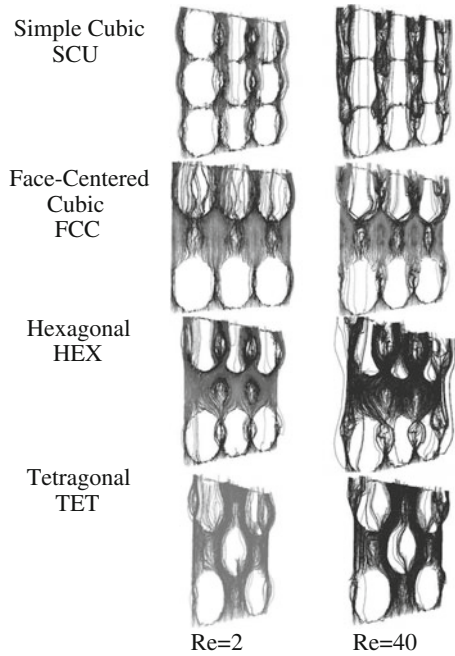


**Table 3** Permeability and inertial coefficient of packing arrangements [60]

Packing model	Porosity	Permeability ( $m^2$ ) $\times 10^{-8}$	Inertial coefficient (1/m)
SCU	0.58	3.40	1650
FCC		1.82	2525
ORT		2.24	2241
HEX		3.20	1795
RHE		2.12	2277
TET		1.93	2496

particles was also evaluated [59, 60]. Particles (density 200 and 2000  $kg/m^3$ , diameters between 0.2 and 10  $\mu m$ ) are released at the inlet of the packing structure and tracked through the structure until they are trapped on the solid beds or escape through the outlet of the structure. The results are shown in Tables 4 and 5. For light particles, Reynolds number plays the major role in fractional penetration of particles (the effect of size is negligible). Besides, heavy and big size particles (i.e., particles with large inertia) have a better chance to get escape from packing structures SCU and HEX due to the existence of well-defined preferential channels of fluid flow that enable particles to cross these structures without contact with solid spheres.

**Table 4** Fractional penetration of particles per solid sphere  $\Pi$  (particles density 200 kg/m<sup>3</sup>) [60]

Packing model	$Re_D (= \rho u d_{est} / \mu)$					
	0.2			40		
	Particles size ( $\mu\text{m}$ )			Particles size ( $\mu\text{m}$ )		
	0.2	2	10	0.2	2	10
	$\Pi$			$\Pi$		
SCU	0.025	0.025	0.025	0.028	0.029	0.031
FCC	0.027	0.027	0.028	0.030	0.031	0.032
HEX	0.027	0.027	0.028	0.030	0.031	0.032
RHE	0.028	0.028	0.028	0.032	0.032	0.033
TET	0.027	0.027	0.028	0.030	0.031	0.031

**Table 5** Fractional penetration of particles per solid sphere  $\Pi$  (particles density 2000 kg/m<sup>3</sup>) [60]

Packing model	$Re_D (= \rho u d_{est} / \mu)$					
	0.2			40		
	Particles size ( $\mu\text{m}$ )			Particles size ( $\mu\text{m}$ )		
	0.2	2	10	0.2	2	10
	$\Pi$			$\Pi$		
SCU	0.025	0.025	0.026	0.029	0.030	0.032
FCC	0.027	0.027	0.027	0.031	0.032	0.023
HEX	0.027	0.028	0.028	0.031	0.031	0.035
RHE	0.027	0.028	0.028	0.032	0.034	0.026
TET	0.027	0.027	0.028	0.031	0.032	0.020

## 9 Bio-Inspired T-Shaped Filters

T-shaped structures with circular and square cross-section were studied by Serrenho and Miguel [58]. The geometric characteristics are presented in Table 6.

A Lagrangian approach to solid suspensions representation was used to obtain the fractional penetration of particles in the T-shaped structures (Table 7). It is observed that this quantity is almost not affected both by the geometry (R, RHM, S and SHM) and the Reynolds number. The penetration of particles is determined by the size of the particles.

## 10 Filter Design from Theory

Flow systems achieve high performance by acquiring a suitable design (configuration). Therefore, improving filter design is a key issue. A major step toward making system design a science is provided by the Constructal law of Adrian

**Table 6** Geometric characteristics of symmetric T-shaped structures (Fig. 13): (R) circular cross-section, (S) square cross-section; (HM) designed based on Hess-Murray law of physiology [5]. Area covered by each structure 57.2 cm<sup>2</sup> and total volume of each structure 2.4 cm<sup>3</sup> [58]

Tube geometry		d <sub>1</sub> (cm)	d <sub>2</sub> , d <sub>3</sub> (cm)	L <sub>1</sub> (cm)	L <sub>2</sub> , L <sub>3</sub> (cm)
Round	R	0.44	0.44	5.35	5.35
	RHM	0.50	0.40	6.00	4.76
Square	S	0.44	0.44	5.35	5.35
	SHM	0.45	0.36	6.00	4.76

**Table 7** The fractional penetration of particles versus the particle diameter [58]

Re	R, RHM d <sub>p</sub> (μm)				S, SHM d <sub>p</sub> (μm)			
	0.1	10	50	100	0.1	10	50	100
20	0.90	0.93	0.45	0.00	0.89	0.88	0.35	0.01
40	0.91	0.93	0.10	0.00	0.90	0.87	0.09	0.01
60	0.90	0.92	0.01	0.00	0.89	0.88	0.03	0.00
80	0.90	0.90	0.00	0.00	0.89	0.86	0.02	0.00

Bejan [4, 3, 43–37, 38]. This law states that if a system is free to morph under global constraints, the better flow design is the one that minimizes the global flow resistances, or maximizes the global flow access. Therefore, design matters and shouldn't be developed by chance.

The challenge is to design a high efficiency filter for the capture of submicrometre particles. The filter operates at low Reynolds numbers (laminar flow) and due to practical and economic reasons it must fit in a fixed volume (the global constraint). The purpose of the filter is to maximize deposition rate, or said in another way, is to have the smallest concentration possible of particles at the outlet.

Consider that the collecting elements of the filter (of cross-section YW) are smooth tubes with characteristic length d. If  $\phi$  is the porosity of the stack then the space allocated to the device permits the installation of  $\varepsilon (= \phi YW/0.25\pi d^2)$  tubes. While a large area available for the deposition of particles is desirable, the resulting penalty on fluid flow resistance is undesirable (see Sect. 5). Therefore the optimal d results from the competition between the number of tubes for large particle deposition and increasing flow resistance. The methodology presented by Reis et al. [54] is developed in two steps: finding the limits, small-d and large-d behaviour and identifying the d-value that maximizes particles' deposition within the filter. The optimal ratio d/H is given by

$$\left(\frac{d}{H}\right)_{\text{optimal}} = 3.44 \frac{\phi^{2/3}}{Be^{2/7}} \left(\frac{H}{W}\right)^{1/7} \tag{29}$$

with

$$Be = \frac{H^2 \Delta p}{\mu D_{df}}$$

Here  $Be$  is the Bejan number,  $D_{df}$  is the diffusion coefficient,  $H$  is the thickness and  $W$  is the filter width.

Another relevant situation is the optimization of granular and fibrous filters. Consider a filter that has porosity  $\phi$  and contains  $N$  collector elements (i.e. fibres, beds) with a characteristic transversal dimension  $d_K$ . This material is mounted on a cylindrical frame of volume  $V$ . Two far-off situations are considered: collector elements are very close to each other and collector elements sufficiently far apart. The optimal geometry is Reis et al. [54]

$$\left(\frac{d_K}{H}\right)_{optimal} = \left[ \frac{\lambda_K}{\lambda_\phi} \frac{\phi^3}{(1-\phi)^3} Be \right]^{1/2} \quad (30)$$

or

$$\phi_{optimal} = \frac{\Lambda^{1/3}}{1 + \Lambda^{1/3}} \quad (31)$$

with

$$\Lambda = \frac{\lambda_\phi d_K}{\lambda_K H Be}$$

where  $\lambda_\phi$  and  $\lambda_K$  are parameters that depend on the geometric arrangement (e.g., for a cubic packing are 180 and 12, respectively).

Consider now a filter with a bio-inspired design (tree-shaped or T-shaped flow structure) which the area covered by the geometry and the total volume allocated to the piping system are kept constant (the global constraint). In this design each segment (parent) gives rise to two daughter branches (Fig. 13). The minimum flow resistance is achieved if the diameters and the lengths of consecutive pipes in a bifurcation are related as [39, 41, 58]

$$d_1^{n_d} = 0.5 \left[ (1 + \lambda_d^{n_d}) d_3^{n_d} + (1 + \lambda_d^{-n_d}) d_2^{n_d} \right] \quad (32)$$

$$L_1^{n_L} = 0.5 \left[ (1 + \lambda_L^{n_L}) L_3^{n_L} + (1 + \lambda_L^{-n_L}) L_2^{n_L} \right] \quad (33)$$

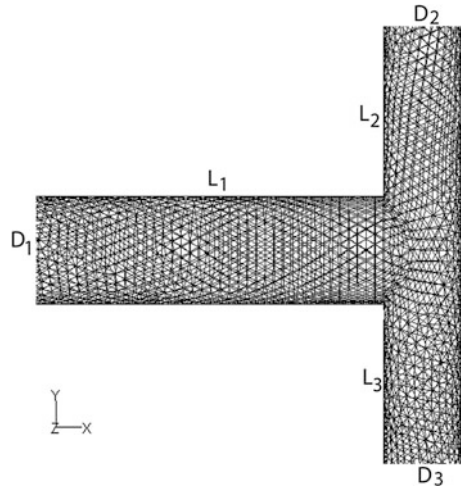
with  $\lambda_d = d_2/d_3$ ,  $\lambda_L = L_2/L_3$ ,  $n_d = n_L = 3$  (laminar flow), and  $n_d = 7/3$  and  $n_L = 7$  (turbulent flow). For symmetric bifurcation pipes ( $\lambda_d = \lambda_L = 1$ ) and laminar flow, these equations become  $d_2/d_1 = L_2/L_1 = 2^{-1/3}$  which are nothing more than the Hess-Murray law of physiology. Using a similar procedure to the previous examples, we obtain (Miguel [39])

$$\left(\frac{d_1}{L_1}\right)_{optimal} = 3.73 \frac{\lambda_{tree}^{3/5}}{Be^{2/5}} \left(\frac{Y^4}{LW^2L_1}\right)^{1/5} \quad (34)$$

where  $L$  is the length of 1st parent segment,  $W$  is the filter width,  $Y$  is the height of the filter and  $\lambda_{tree}$  is a geometry factor that depends of branching level.



**Fig. 13** T-shaped structure that can be used for filtration



In Eqs. (28), (29) and (33) the optimized design of the filter is strongly dependent both on Bejan number and desired void fraction of the filter.

## References

1. ASME: Code on Nuclear Air and Gas Treatment. American Society of Mechanical Engineers ASME AG-1, New York (2003)
2. Aydın, M., Balik, G., Miguel, A.F., Reis, A.H.: Some features of flow and particle transport in porous structures. *J. Mech. Eng.* **51**, 495–500 (2005)
3. Bejan, A.: *Shape and Structure, from Engineering to Nature*. Cambridge University Press, Cambridge (2000)
4. Bejan, A., Lorente, S.: *Design with Constructal Theory*. Wiley, Hoboken (2008)
5. Bejan, A., Dincer, I., Lorente, S., Miguel, A.F., Reis, A.H.: *Porous and Complex Flow Structures in Modern Technologies*. Springer, New York (2004)
6. Bergman, W., Taylor, R.D., Miller, H.H., Biermann, A.H., Hebard, H.D., da Roza, R.A., Lum, B.Y.: Enhanced filtration program at LLNL. In: *Proceedings of 15th DOE Nuclear Air Cleaning Conference (CONF-760822)* Boston (1978)
7. Burganos, V.N., Skouras, E.D., Paraskeva, C.A., Payatakes, A.C.: Simulation of the dynamics of depth filtration of non-Brownian particles. *AIChE J.* **47**, 880–894 (2001)
8. Costa, D.L., Kodavanti, U.P.: Toxic responses of the lung to inhaled pollutants: benefits and limitations of lung-disease models. *Toxicol. Lett.* **140–141**, 195–203 (2003)
9. Dales, R., Chen, L., Frescura, A.M., Liu, L., Villeneuve, P.J.: Acute effects of outdoor air pollution on forced expiratory volume in 1 s: a panel study of schoolchildren with asthma. *Eur. Respir. J.* **34**, 316–323 (2009)
10. Davies, C.N.: *Air Filtration*. Academic Press, London (1973)
11. Dominici, F., Peng, R.D., Bell, M.L., Pham, L., McDermott, A., Zeger, S.L., Samet, J.M.: Fine particulate air pollution and hospital admission for cardiovascular and respiratory diseases. *J. Am. Med. Assoc.* **295**, 1127–1134 (2006)
12. D’Ottavio, T., Goren, L.S.: Aerosol capture in granular beds in the impaction dominated regime. *Aerosol Sci. Technol.* **2**, 91–108 (1983)

13. Durant, W.S.: Performance of Airborne Activity Confinement Systems in the Savannah River Plant Reactor Buildings. USAEC Report CONF-660904 (1966)
14. Emi, H., Wang, C.S., Tien, C.: Transient behavior of aerosol filtration in model filters. *AIChE J.* **28**, 397–405 (1982)
15. Ergun, S.: Fluid flow through packed columns. *Chem. Eng. Progr.* **48**, 89–94 (1952)
16. First, M.W., Gilbert, H.: Aerosol filtration. *Nucl. Saf.* **2**, 167–175 (1982)
17. Flagan, R.C., Seinfeld, J.H.: *Fundamentals of Air Pollution Engineering*. Prentice-Hall, Englewood Cliffs (1988)
18. Gautam, A., Waldrep, J.C., Densmore, C.L.: Aerosol gene therapy. *Mol. Biotechnol.* **23**, 51–60 (2003)
19. Gilbert, H.: High-Efficiency Particulate Air Filter Units, Inspection, Handling, Installation. AEC Report TID-7023, National Technical Information Service, Springfield (1961)
20. Griesenbach, U., Ferrari, S., Geddes, D.M., Alton, E.W.: Gene therapy progress and prospects: cystic fibrosis. *Gene Ther.* **9**, 1344–1350 (2002)
21. Hinds, W.C.: *Aerosol Technology*. Wiley, New York (1982)
22. Hosseini, S.A., Tafreshi, H.V.: Modeling particle-loaded single fiber efficiency and fiber drag using ANSYS–Fluent CFD code. *Comput. Fluids* **66**, 157–166 (2012)
23. Jaenicke, R.: Abundance of cellular material and proteins in the atmosphere. *Science* **308**, 73 (2005)
24. Joubert, A., Laborde, J.C., Bouilloux, L., Callé-Chazelet, S., Thomas, D.: Influence of humidity on clogging of flat and pleated HEPA Filters. *Aerosol Sci. Technol.* **44**, 1065–1076 (2010)
25. Joubert, A., Laborde, J.C., Bouilloux, L., Callé-Chazelet, S., Thomas, D.: Modelling the pressure drop across HEPA filters during cake filtration in the presence of humidity. *Chem. Eng. J.* **166**, 616–623 (2011)
26. Jung, Y., Tien, C.: New correlations for predicting the effect of deposition on collection efficiency and pressure drop in granular filters. *J. Aerosol Sci.* **22**, 187–200 (1991)
27. Kockmann, N., Dreher, S., Engler, M., Woias, P.: Simulation and characterization of microreactors for aerosol generation. *Microfluid. Nanofluid.* **3**, 581–589 (2007)
28. Krcma, R.: *Manual of Nonwovens*. Textile Trade Press, Manchester (1971)
29. Langmuir, I.: *Report on Smokes and Filters*, OSRD 865. Office of Scientific Research and Development, Office of Technical Services, Washington (1942)
30. Lapple, C.E.: *Deep Bed Sand and Glass Fiber Filters*. USAEC Report WASH 149 (1952)
31. Mackenzie, D.: The proof is in the packing. *Am. Sci.* **86**, 1 (1998)
32. McCarthy, M.W.: Trivalent intranasal influenza vaccine, live. *Ann. Pharmacother.* **38**, 2086–2093 (2004)
33. Mercimek, M., Yildirim, H., Miguel, A. F., Aydin, M.: Investigation of T-shape geometry for the collection of pollution particles. In: Dincer, I., Colpan, C.O., Midilli, A. (eds.) *Proceedings of the Global Conference on Global Warming 2009*, pp. 1172–1179 (2009)
34. Miguel, A.F.: Airflow through porous screens: from theory to practical considerations. *Energy Build.* **28**, 63–69 (1998)
35. Miguel, A.F.: Effect of air humidity on the evolution of permeability and performance of a fibrous filter during loading with hygroscopic and non-hygroscopic particles. *J. Aerosol Sci.* **34**, 783–799 (2003)
36. Miguel, A.F.: Porous media and filtration. In: Ingham, D.B., Bejan, A., Mamut, E., Pop, I. (eds.) *Emerging Technologies and Techniques in Porous Media*, pp. 419–431. Kluwer Academic Publishers, Dordrecht (2004)
37. Miguel, A.F.: Dendritic structures for fluid flow: laminar, turbulent and constructal design. *J. Fluids Struct.* **26**, 330–335 (2010)
38. Miguel, A.F.: Natural flow systems: acquiring their constructal morphology. *Int. J. Des. Nat. Ecodev.* **5**, 230–241 (2010)
39. Miguel, A.F.: Tree-shaped flow structures viewed from the constructal theory perspective. In: Dias, R., Martins, A.A., Lima, R., Mata, T.M. (eds.) *Single and Two-Phase Flows on*

- Chemical and Biomedical Engineering, pp. 266–291. Bentham Science Publishers, Oak Park (2012)
40. Miguel, A.F.: Non-darcy porous media flow in no-slip and slip regimes. *Therm. Sci.* **16**, 167–17 (2012)
  41. Miguel, A.F.: Lungs as a natural porous media: architecture, airflow characteristics and transport of suspended particles. In: Delgado, J.M.P.Q. (ed.) *Heat and Mass Transfer in Porous Media*, pp. 115–137. Springer, Berlin (2012)
  42. Miguel, A.F., Silva, A.M.: Experimental study of mass loading behaviour of fibrous filters. *J. Aerosol Sci.* **32**(S1), 851–852 (2001)
  43. Miguel, A.F.: Computational analysis of the role of permeability and inertia on fluid flow through porous media. In: Delgado, J.M.P.Q. (ed.) *Current Trends in Chemical Engineering*, pp. 1–19. Studium Press LLC, Houston (2010)
  44. Miguel, A.F., Reis, A.H.: Transport and deposition of fine mode particles in porous filters. *J. Porous Media* **8**, 731–744 (2006)
  45. Miguel, A.F., Reis, A.H., Melgão, M.: Urban indoor-outdoor aerosol measurements in Portugal and the global warming scenario. *Int. J. Global Warming* **1**, 356–367 (2009)
  46. Mikszta, J.A., Sullivan, V.J., Dean, C., Waterston, A.M., Alarcon, J.B., Dekker III, J.P., Brittingham, J.M., Huang, J., Hwang, C.R., Ferriter, M., Jiang, G., Mar, K., Saikh, K.U., Stiles, B.G., Roy, C.J., Ulrich, R.G., Harvey, N.G.: Protective immunization against inhalational Anthrax: a comparison of minimally invasive delivery platforms. *J. Infect. Dis.* **191**, 278–288 (2005)
  47. NAAQS.: The national ambient air quality standards for particle pollution: summary of proposed improvements to air quality standards for particle pollution and updates to the air quality index <http://www.epa.gov/pm/2012/fsstandards.pdf> (2012). Accessed 18 Oct 2012
  48. NCEA.: Air quality criteria for particulate matter. National Center for Environmental Assessment, US Environmental Protection Agency, Research Triangle Park, NC (2004)
  49. Payet, S., Boulaud, D., Madelaine, G., Renoux, A.: Penetration and pressure drop of a HEPA filter during loading with submission liquid particles. *J. Aerosol Sci.* **23**, 723–735 (1992)
  50. Pope, C.A., Burnett, R.T., Thurston, G.D., Thun, M.J., Calle, E.E., Krewski, D., Godleski, J.J.: Cardiovascular mortality and long-term exposure to particulate air pollution: epidemiological evidence of general pathophysiological pathways of disease. *Circulation* **109**, 71–77 (2004)
  51. Quigley, C., Easter, C., Burrowes, P.: Biotechnology-based odour control: design criteria and performance data. *Water Sci. Technol.* **50**, 319–326 (2004)
  52. Quintard, M., Whitaker, S.: Aerosol filtration: an analysis using the method of averaging volume. *J. Aerosol Sci.* **26**, 1227–1255 (1995)
  53. Rege, S.D., Fogler, H.S.: A network model for deep bed filtration of solid particles and emulsion drops. *AIChE J.* **11**, 1761–1772 (1988)
  54. Reis, A.H., Miguel, A.F., Bejan, A.: Constructal theory of particle agglomeration and design of air-cleaning devices. *J. Phys. D* **39**, 2311–2318 (2006)
  55. Riddle, A., Carruthers, D., Sharpe, A., McHugh, C., Stocker, J.: Comparisons between FLUENT and ADMS for atmospheric dispersion modeling. *Atmos. Environ.* **38**, 1029–1038 (2004)
  56. Rudel, R.A., Camann, D.E., John D. Spengler, J.D., Leo R. Korn, L.R., Julia, G., Brody, J.G.: Alkylphenols, pesticides, phthalates, polybrominated diphenyl ethers, and other endocrinedisrupting compounds in indoor air and dust. *Environ. Sci. Technol.* **37**, 4543–4553 (2003)
  57. Schmidt, E.W.: Filtration of aerosols in granular bed. *J. APCA* **28**, 143–157 (1978)
  58. Serrenho, A., Miguel, A. F.: Accessing the influence of Hess-Murray law on suspension flow through ramified structures. *Defect and Diffusion Forum* **334**, 322–328 (2013)
  59. Serrenho, A., Miguel, A.F.: Simulation and characterization of high porosity media for aerosol particle processing. *J. Porous Media* **12**, 1129–1138 (2009)
  60. Serrenho, A., Miguel, A.F.: Fluid flow and solid/fluid suspensions flow in 3-D packed beds of spheres: the effect of periodicity of fixed beds. *Defect Diffus. Forum* **315**, 871–876 (2011)

61. Shapiro, M., Brenner, H.: Dispersion/reaction model of aerosol collection by porous filters. *J. Aerosol Sci.* **21**, 97–125 (1990)
62. Shapiro, M., Brenner, H.: Dispersion/reaction model of aerosol collection by porous filters. *J. Aerosol Sci.* **21**, 97–125 (1990)
63. Shareefdeen, Z., Singh, A.: *Biotechnology for Odor and Air Pollution Control*. Springer, New York (2005)
64. Shoeib, M., Harner, T., Ikonou, M., Kannan, K.: Indoor and outdoor air concentrations and phase partitioning of perfluoroalkyl sulfonamides and polybrominated diphenyl ethers. *Environ. Sci. Technol.* **38**, 1313–1320 (2004)
65. Spurny, K.R.: *Advances in aerosol filtration*, CRC Press LLC, Florida (1997)
66. Stockdale, W.G., Suddath, J.C., Eister, W.K.: Control of radioactive air contamination at Oak Ridge National Laboratory. In: *Proceedings of 3rd Atomic Energy Commission Air Cleaning Conference*, pp. 55–57, Los Alamos, NM. (1950)
67. Tien, C.: *Granular Filtration of Aerosols and Hydrosols*. Butterworths, Boston (1989)
68. USEPA.: National ambient air quality standards for particulate matter. US Environmental Protection Agency. *Fed Regist* **62**, 138. [http://www.epa.gov/ttn/caaa/t1/fr\\_notices/pmnaaqs.pdf](http://www.epa.gov/ttn/caaa/t1/fr_notices/pmnaaqs.pdf) 1997. Accessed 18 Oct 2012
69. Wadsworth, L.C., Hutten, I.M.: *Handbook of Nonwoven Filter Media*. Elsevier, Oxford (2007)
70. Wepfer, R.: Characterisation of HEPA and ULPA filters by proposed new European test methods. *Filtr. Sep.* **32**, 545–550 (1995)
71. Yadav, N., Morris, G., Harding, S.E., Ang, S., Adams, G.G.: Various non-injectable delivery systems for the treatment of diabetes Mellitus. *Endocr. Metab. Immune Disord. Drug Targets* **9**, 1–13 (2009)
72. Zhao, Z.M., Tardos, G., Pfeffer, R.: Separation of airborne dust in electrostatically enhanced fibrous filters. *Chem. Eng. Commun.* **108**, 307–332 (1991)